Eidgenössische Technische Hochschule Zürich
Swiss Federal Institute of Technology Zurich

Empa
Materials Science and Technology

Fatigue Behavior Investigation of Additively Manufactured Ti-6Al-4V

Research Project

Alexander Gillmann

Advisor: Dr. Ehsan Hosseini

September 2019

Acknowledgements

I would like to give special thanks to my supervisor Dr. Ehsan Hosseini for always instructing me and for answering my questions with patience. I also would like to thank Daniele Ghedalia and Serjosha Robmann for helping me to build the fatigue test setup. Furthermore, I am also very thankful for the help of Xiaolong Li with the microscopic analysis.

Contents

Chapter 1

Introduction

Titanium (Ti) and its alloys, including Ti-6Al-4V which has been investigated during this project, are commonly used as a metallic biomaterial for the manufacturing of orthopedic implants. Examples for such medical applications are hip and spine implants. The properties of Ti alloys which allow this medical usage are high biocompatibility, ductility and corrosion resistance and a high stiffness to weight ratio. However, these properties do not guarantee excellent performance when the implant is substituted into the human skeleton. Implants which replace bone should not only contribute to the stability as an equally shaped substitute, but should also represent similar mechanical response to the substituted bone when a force is applied. The difference in rigidity (and therefore in mechanical behavior) between Ti-6Al-4V (Young's modulus of approximately 110 GPa [1]) and the surrounding bone tissues (0.76-18.2 GPa for trabecular and 4.89-25.8 GPa for cortical bone tissues [1]) can lead to *stress shielding*. Stress shielding occurs within a composite material with a mismatch in rigidity between its components (e. g. one stiff and one flexible component) which is subjected to a mechanical load. In the case of medical implants, where the difference in rigidity between the stiff Ti-6Al-4V structure and the surrounding flexible bone tissue is high, stress shielding leads to shear stresses at the alloy-bone interface and therefore to implant loosening. By lowering the stiffness of the implant, the load transfer to the bone tissues can be improved [1] which reduces the risk of bone resorption. Stress shielding also has an effect on bone remodeling as well as on the healing process of the bone tissue [2].
The modulus of a structure does not only depend on the material, but also on its topology. In order to lower stress shielding and bone resorption, the idea was to increase the porosity of the implant material such that the nodes are ordered periodically within the structure. These porous structures are called *lattice* or *cellular* structures. The advantage of biomedical implants with lattice architectures is that the bone can grow into the metal scaffold which supports bone tissue regeneration. The investigation of metal lattices yielded that the dependence of the modulus of the cellular material on the relative density exhibits a power law behavior [1]:

$$E_s = E_0 \alpha \left(\frac{\rho_s}{\rho_0} \right)^{\beta} \tag{1.1}$$

In eq. (1.1), E_s and E_0 are the moduli of the cellular and the bulk structure, respectively. Analogously, ρ_s and ρ_0 are the densities of the cellular and the bulk material, respectively. The parameters α and β can be determined using finite element mod-

eling (FEM). Chen et al. [1] performed FE calculations for Ti lattices and obtained $\beta = 2$. Since β is positive, one can see by following eq. (1.1) that the modulus of the Ti lattice decreases if its density decreases. Tunable stiffness of metal lattices for biomedical applications is valuable. An advantage of these lattice structures is that they are osteoconductive, meaning that bones can grow into the metal scaffold. This is an important aspect since the ability to grow into the lattice pores facilitates bone tissue regeneration [3]. Since the sufficient porosity levels cannot be achieved with the powder sintering route, additive manufacturing (AM) (also known as 3D printing) methods such as selective laser melting (SLM) or electron beam melting (EBM) methods have been used to fabricate lattice structures with a stiffness similar to bone tissues. The specimens that were investigated during this research project were manufactured via SLM. In the SLM method, metal powder layers are formed and, based on a CAD file, are selectively melted using laser irradiation [4]. AM techniques allow the production of structures with complex microarchitectures for patient-specific implants. Due to the stress distribution in human bone tissues, the density of bone varies and the stiffness becomes a rather local property. Another advantage of AM is that it provides the tools to fabricate graded stiffness implants that exhibit the same position-dependent change in stiffness as bone tissues [1].
The performance of SLM Ti-6Al-4V hip implants has already been tested by installing it to a patient [4]. The patient was capable of moving with the installed implant.
Although these lattice structures fulfil the conditions for the usage as implants, there are some limitations and difficulties that come along with AM. First of all, the strut thickness of lattices is limited to 200 μm for most of the currently used AM methods [5]. A limited strut thickness means that the ratio between surface and volume in the structure is limited. Since the surface area determines the amount of bone ingrowth into the lattice, bone ingrowth can only be improved to a certain extent. Another disadvantage of AM is that deviations from the designed structure occur in the manufactured parts. Differences in strut thickness, strut cross section shape or porosity can occur [5]. During the fabrication of AM lattice structures, a high amount of imperfections such as notches, lack of fusion (LOF) defects, undesired strut porosity or a high surface roughness is induced. LOF defects are cavities that can contain unmelted powder particles, but this is not always the case. Since the magnitude of the stress is increased (*stress concentration effect*) in the vicinity of such discontinuities, these imperfections lower the fatigue endurance of the structure.
I now want to explain the effects of various parameters on the fatigue performance of lattice structures:

- *Print orientation*: Qianchu et al. [6] performed fatigue tests at two stress levels, 600 MPa and 700 MPa, for horizontally as well as vertically printed SLM Ti-6Al-4V specimens. The average fatigue lifetimes of the horizontal specimens were higher for both stress levels. The print orientation determines the orientation of LOF defects with respect to the loading direction. LOF defects are primarily formed between subsequently deposited layers and are therefore aligned perpendicular to the printing direction. That means that the effective crack size is higher in the vertical specimens, resulting in an inferior average fatigue endurance.

- *Stress ratio* or *R-ratio*, defined as the ratio R = $\sigma_{min}/\sigma_{max}$, where σ_{min} and σ_{max} are the minimum and maximum stress in a stress cycle: The fatigue endurance decreases with increasing stress amplitude, which is given by

$$\sigma_{amp} = \sigma_{max}\left(\frac{1-R}{2}\right) \tag{1.2}$$

  Using eq. (1.2), one can determine how the stress amplitude changes when changing R for a given $\sigma_{max} > 0$. For this, it is important to mention that it always holds that $\sigma_{amp} > 0$. The mean stress reads

$$\sigma_m = \sigma_{amp} + R \cdot \sigma_{max} = \left(\frac{1+R}{1-R}\right)\sigma_{amp} \tag{1.3}$$

  According to eq. (1.3), the mean stress increases if R increases for a constant value of σ_{amp}. An increasing mean stress yields a reduction of the fatigue endurance since tensile forces are contributing more to fatigue failure than compressive forces.

- *Post-treatment*: As an example, surface modification methods like chemical etching can be used to decrease the surface roughness. Chemical etching also decreases the thickness of the struts in a scaffold, which can lead to a higher lattice porosity. In a recent study [7], it was found out that chemical etching indeed increases the fatigue limit of EBM Ti-6Al-4V struts when compared to the as-built specimens.

When the lattice implant is installed into the body, the bone tissues start to regenerate through bone ingrowth. The tissue-lattice composite differs in mechanical behavior from the sole metal lattice. Hedayati et al. [8] filled Ti-6Al-4V lattice samples with different porosity values with epoxy to simulate the from the bone ingrowth resulting structure. Fatigue tests were performed for the filled samples and it turned out that, for every porosity level, the filled structure was stronger in fatigue than the unfilled structure. The fatigue strengths increased by factors 2-8, were the highest factor was observed for the highest-porosity structure.

Chapter 2

Materials and Methods

2.1 Material

All struts and lattices that were tested during this project have been fabricated by the British company Renishaw plc. To produce the specimens, an AM250 system with a laser power of 200 W was used. The layer thickness of the Ti-6Al-4V powder was 30 μm. The printed specimens were annealed for two hours at 850°C ± 10°C. No post-treatments like hot isostatic pressing (HIP) or surface modification have been applied.

2.1.1 Strut Specimens

The strut specimens that I tested during this project were printed *diagonally*, meaning that the angle between the strut axis and the printing direction is equal to 45°. The diameters of the struts were in the range of 200 to 300 μm with a high variation. Furthermore, I analyzed data that has been obtained from fatigue tests for vertically printed struts. These tests were performed during a previous project done in the group. I took the minimum diameters of the struts to calculate an upper bound for the stress amplitudes that were applied during the fatigue tests.

2.1.2 Lattice Specimens

All lattices under investigation were printed *vertically* with a 0° angle between the lattice axis and the printing direction. All lattices had a tetrahedron cell topology.

2.2 Fatigue Testing

2.2.1 Strut Testing

A planar biaxial machine with horizontally mounted hydraulic actuators, a hydraulic power unit and 100 N load cells (MTS Systems, Eden Prairie, USA) have been used to conduct all fatigue tests. The strut samples were clamped between two fixtures and were aligned manually such that the strut axis is approximately parallel to the direction of the applied force. It cannot be assured that the clamping length was the same for all specimens, and it is recommended to take a measurement to assure similar clamping lengths for future testing. Only one axis was moving while the

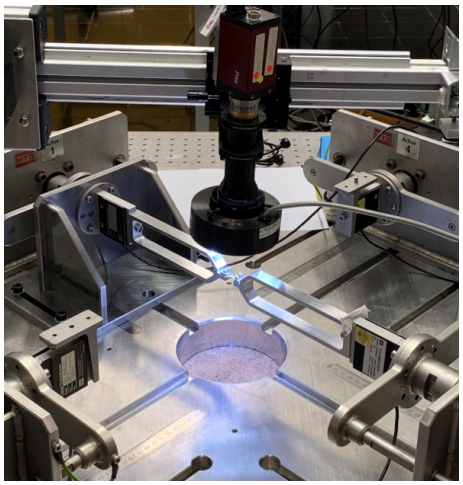

Figure 2.1: Test setup for struts

other axis was static. All strut specimens were tested in tension-tension load mode at a constant R-ratio of 0.1 and a frequency of 10 Hz. A fatigue test was stopped if the sample failed or if the number of applied stress cycles exceeded 10^6 (*runout*). Fig. 2.1 shows the fatigue test setup for struts with a clamped strut specimen.

2.2.2 Lattice Testing

A servohydraulic test system with a 100 kN load cell (MTS Systems, Eden Prairie, USA) was used to perform uniaxial fatigue tests for vertical lattices. The test setup with a clamped lattice can be seen in Fig. 2.2. Some of the lattices were tested in tension-tension load mode for a R-ratio of 0.1 during a previous project in the group. During my project, I tested lattices in tension-compression load mode for a R-ratio of -1. In all performed fatigue tests for lattices, the frequency was set to 10 Hz. In a previous study, an equivalent area of the lattices has been determined using elastic linear finite element analysis. This equivalent area is equal to the cross-sectional area that would yield the same E-modulus as that of bulk Ti-6Al-4V.

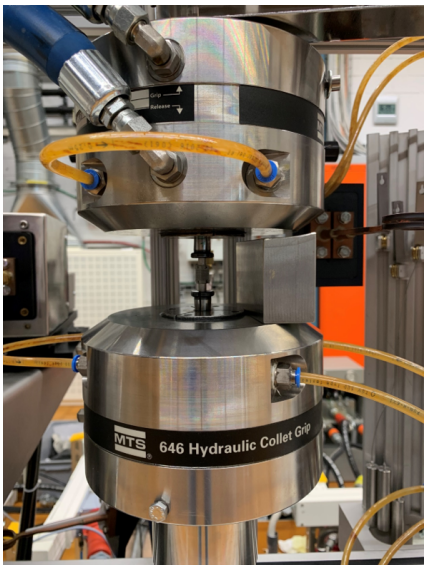

Figure 2.2: Test setup for lattices

2.2.3 Scanning Electron Microscope (SEM) Analysis

In order to see if there is any correspondence between lifetime and fracture behavior and to investigate the fracture surfaces of lattices that were tested for different values of the R-ratio, a scanning electron microscope (SEM) was used to have a closer look at the fracture surfaces of tested strut and lattice specimens.

Chapter 3

Results

3.1 Fatigue Test Results

3.1.1 Test Results of Struts

In order to investigate the fatigue behavior of single Ti-6Al-4V struts, different stress amplitudes have been applied in the tests. Fig. 3.1 shows the data that was obtained from the fatigue tests of diagonal and vertical struts and also the fitting curves. For the fits, relations of the form

$$\sigma_{amp}(N) = a \cdot N^b + \sigma^* \tag{3.1}$$

have been used, where σ^* is the estimated fatigue strength of the struts. This value was estimated using the obtained data points. As can be seen from Fig. 3.1, the strut fatigue endurances show a large scatter. For similar stress amplitudes, the endurance varies in average by a factor of 10, which is high considering the fact that the test setup was almost the same for all struts. Especially the diagonal struts exhibit a strange fatigue endurance response, as can be seen by the low coefficient of determination in Fig. 3.1, indicating a very poor fit. For both types of struts, the large scatter might be due to the different amounts of pre-existent defects. Not only the number of defects, but also their orientations with respect to the loading direction, which is also a factor that influences crack initiation, may be different for struts with different built directions. Since the alignment of the struts in the test setup was not ideal, the struts were exposed to additional bending forces, which might be different for each strut. Bending forces also occur if the specimen is curved due to residual stresses, which was the case for some of the tested struts. Fig. 3.1 also shows that the fatigue performances of diagonal and vertical struts are comparable.

For all of the tested struts, the displacement range for each stress cycle (*D-N curves*) was plotted in order to reveal the behavior of the crack growth. Cracks can grow slowly or fast and the rate of the crack growth can be qualitatively determined using the D-N curve of the fatigue test. Fig. 3.2 shows the D-N curves of all tested diagonal struts. According to the values of the applied stress amplitudes, the struts have been divided into four sets such that the stress amplitudes are similar in each set. The aim was to see whether there is a correspondence between the displacement range and the stress level. Ideally, higher stress amplitudes lead to higher displacement

ranges. However, since the clamping length was not the same in all the tests, this does not hold for the curves shown in Fig. 3.2. A correction has been made to order the curves in this manner: Let $\Delta\mathbf{x}$ be the vector that contains all values of the displacement range of one fatigue test for a specific strut. Furthermore, define

$$\Delta x^* = d \cdot \frac{\langle \Delta F \rangle_{100\ cyc.}}{A \cdot E} \tag{3.2}$$

where $d = 2\ mm$ is the length of the strut, which is the reference length for the displacement in the corrected displacement range, $\langle \Delta F \rangle_{100\ cyc.}$ is the average of the difference of the maximum and the minimum force for the first 100 applied cycles, A is the minimum cross-sectional area of the strut and $E = 110$ GPa is the elastic modulus of Ti-6Al-4V. Denote by $\langle \Delta x \rangle_{100\ cyc.}$ the average displacement range for the first 100 cycles, then the corrected displacement range is given by

$$\Delta\mathbf{x}_{corr} = \frac{\Delta\mathbf{x}}{\langle \Delta x \rangle_{100\ cyc.}} \cdot \Delta x^* \tag{3.3}$$

Replacing the average displacement and the average force of the fatigue test by the average values of the initial stiffness check would yield higher accuracy. However, these values were not recorded in this project, but it is recommended for future works. Fig. 3.3 shows the *corrected D-N curves* of the tested diagonal struts. While the correction works well for lower stress levels [Fig. 3.3 (a) and (b)], the curves for higher stress amplitudes [Fig. 3.3 (c) and (d)] are still not ordered.
It can also be seen from Fig. 3.2 that all D-N curves of the diagonal struts are smooth. The rate of crack growth was high for all failed struts.

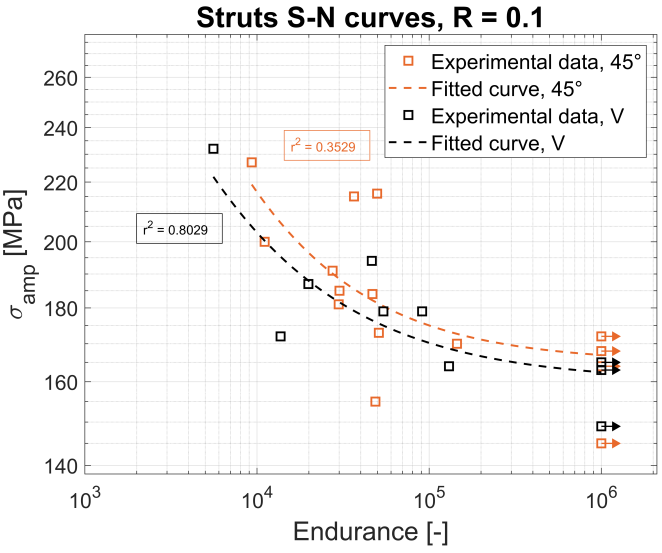

Figure 3.1: Fatigue test data and fitting S-N curves of diagonal and vertical struts. The coefficients of multiple determination of the fits are denoted by r^2. The arrows indicate the runout data.

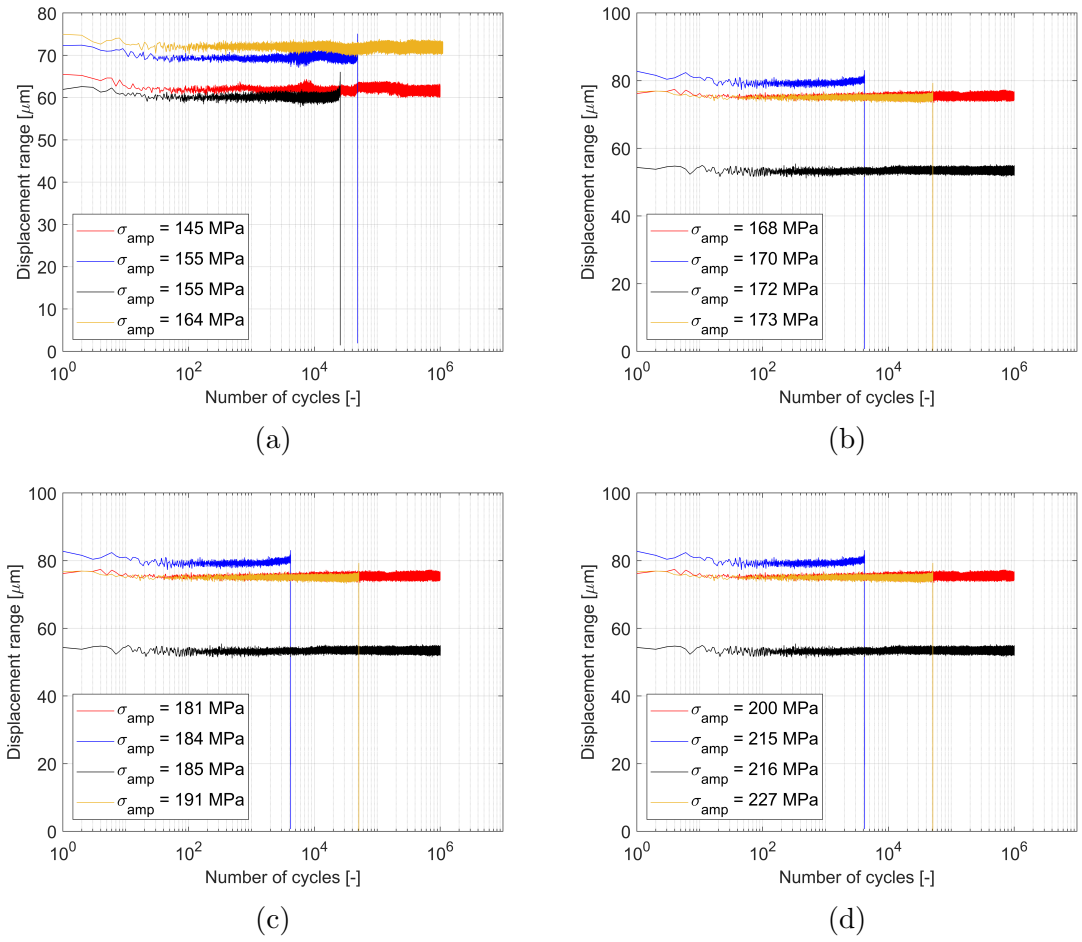

Figure 3.2: Displacement range vs. number of cycles for diagonal struts.

3.1.2 Test Results of Lattices

The fatigue behavior of vertical lattices has been investigated for two different R-ratios, namely for R = 0.1 and R = -1. For the fits, the same relation as for the struts [eq. (3.1)] has been used with the difference that stress has been replaced by force. The fatigue test data and the fitting curves of vertical lattices are shown in Fig. 3.4. The scatter of the fatigue endurance is lower when compared with that of the struts [Fig. 3.1] and the fits describe the dependence of the force amplitude on the endurance better since their coefficients of multiple determination are close to one. For R = -1, the fatigue endurances of the lattices are higher than for R = 0.1. This is due to the lower (tensile) mean force in the cycles for R = -1. Crack initiation and growth that lead to fatigue failure are more sensitive to tensile forces. For the same force amplitude, the amount of tensile forces acting on the lattice per cycle is higher for R = 0.1.

I now want to compare the fatigue performance of the tested vertical lattices to other Ti-6Al-4V structures. Fig. 3.5 (a) shows that the wrought (data taken from [9]) and the bulk AM structures (structure with a machined surface [10] and a HIPed structure with an as-built surface [11]) exhibit better fatigue performances than the tested vertical lattices for R = -1. It can also be seen from Fig. 3.5 (a) that surface machining improves the fatigue performance more than HIP. Also for R = 0.1, the

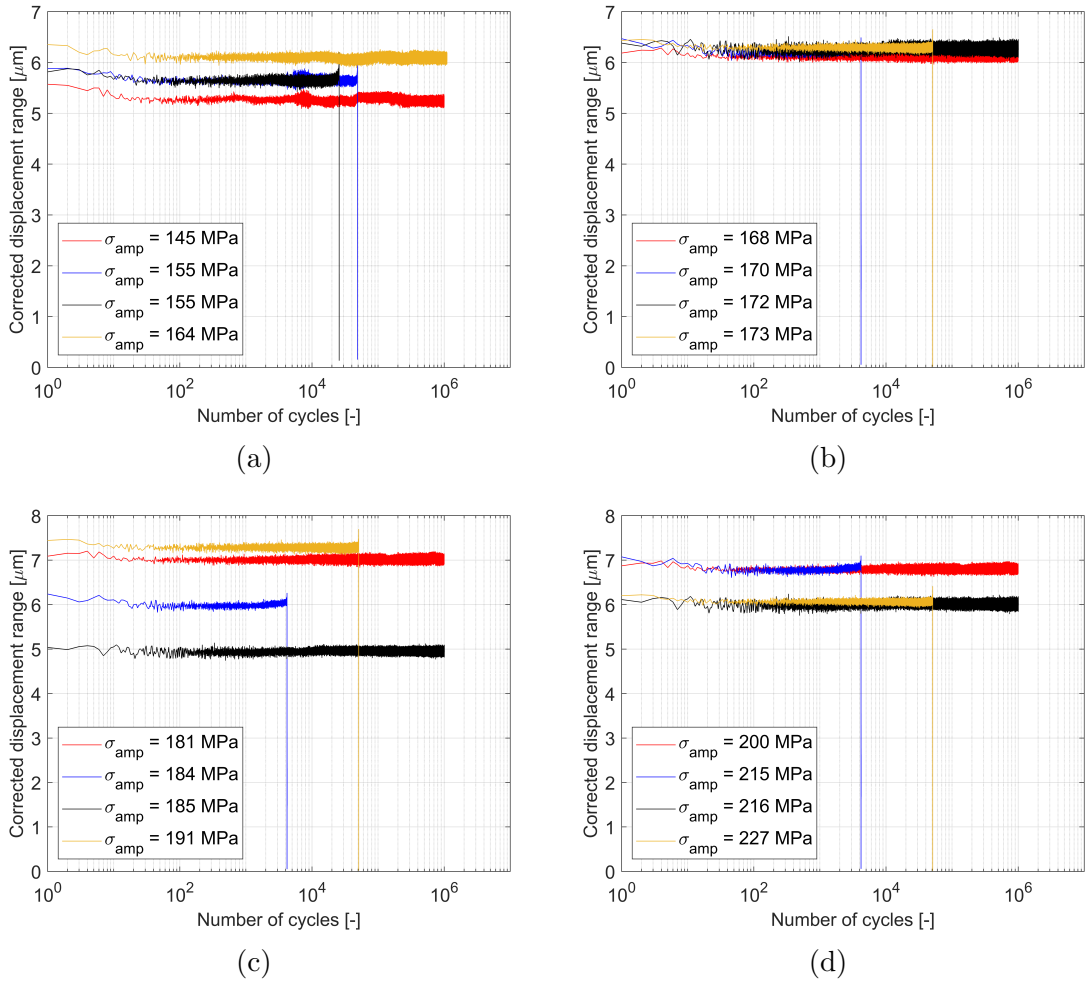

Figure 3.3: Corrected displacement range vs. number of cycles for diagonal struts.

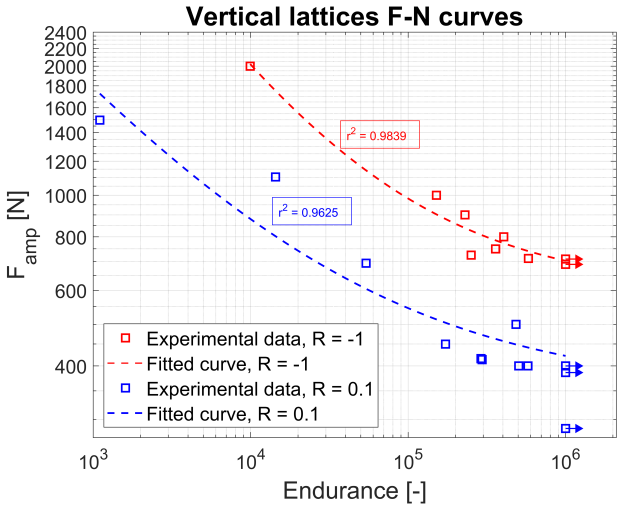

Figure 3.4: Fatigue test data and fitted F-N curves for vertical lattices for the R-ratios R = 0.1 (blue) and R = -1 (red). The coefficients of multiple determination of the fits are denoted by r^2. The arrows indicate the runout data.

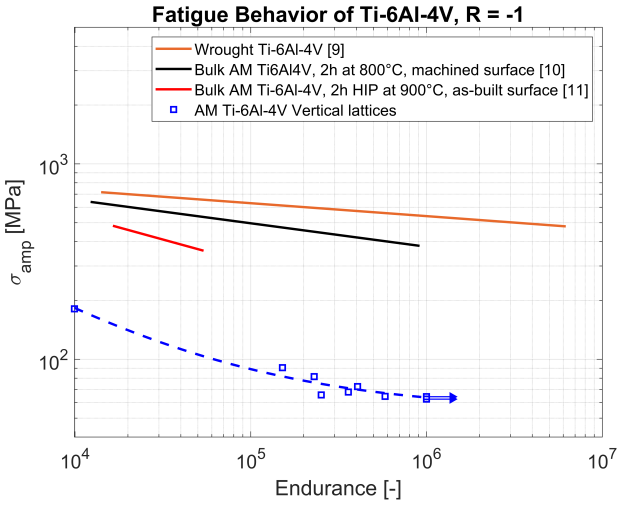

(a)

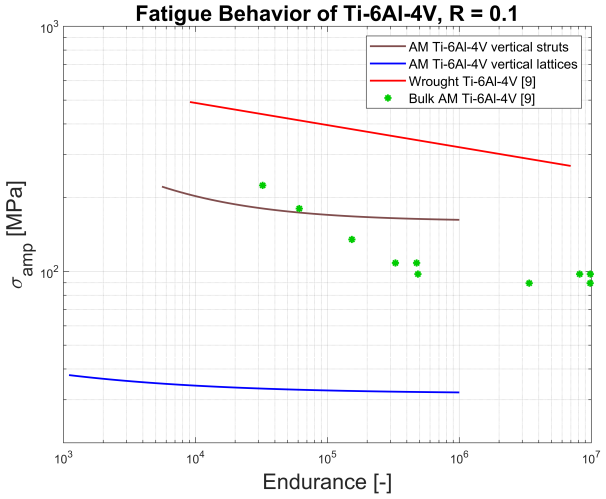

(b)

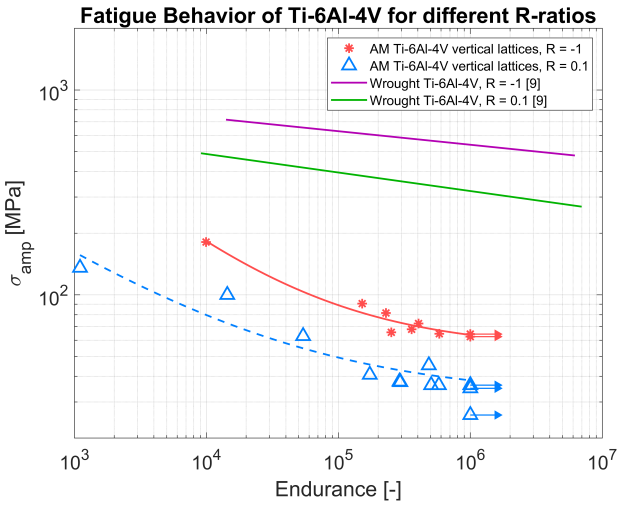

(c)

Figure 3.5: Comparison of fatigue endurance responses of various Ti-6Al-4V structures for constant R-ratios of -1 (a) and 0.1 (b) and for different R-ratios (c). The arrows indicate the runout data.

vertical lattices exhibited lower endurances than other structures, as can be seen from Fig. 3.5 (b). Fig 3.5 (c) compares the fatigue performance of vertical lattices to wrought structures for the two R-ratios R = 0.1 and R = -1. It holds also for the wrought structures that a decreasing R-ratio (and thus a decreasing mean stress) leads to higher fatigue endurances. The as-built lattices are weaker in fatigue than the wrought and bulk AM materials because of the high amount of regions of stress concentration (notches) in the lattices. Fatigue failure initiates mostly from surface defects, e.g. notches, and porous lattices have a much higher (internal) surface area than other materials, making them much more sensitive to a mechanical load.

3.2 SEM Analysis

The fracture surfaces of some of the tested struts and lattices were investigated under the SEM. Three different fracture types were observed: *Transgranular fracture*, *overload dimple rupture* and a *mixed* type. These three fracture types are shown in Fig. 3.6. In the mixed type, regions with transgranular fracture, regions with dimple rupture as well as transition regions co-exist.

3.2.1 Struts

Almost all of the struts failed at one of their transition regions which connect the strut with the other part of the specimen [Fig. 3.7]. The fatigue sensitivity of a notch (*notch sensitivity*) increases with its radius. Although the struts contained a high amount of surface defects, these notches are small compared to the transition region that acts as a real notch. This is the reason why failure occurred mostly at these regions.
I want to compare the fracture behavior of low-cycle fatigue (LCF) diagonal struts to high-cycle fatigue (HCF) diagonal struts (R = 0.1 for all of the struts). First of all, it should be mentioned that big pores were observed in almost all of the fracture surfaces of the struts under investigation. Fig. 3.8 shows the fracture surfaces of a representative LCF strut (number of cycles to failure $N = 2430$) and a HCF strut ($N = 46385$). The LCF struts exhibited a mixed type with approximately the same amount of transgranular fracture and dimple rupture. Mainly transgranular fracture was observed in the HCF strut.

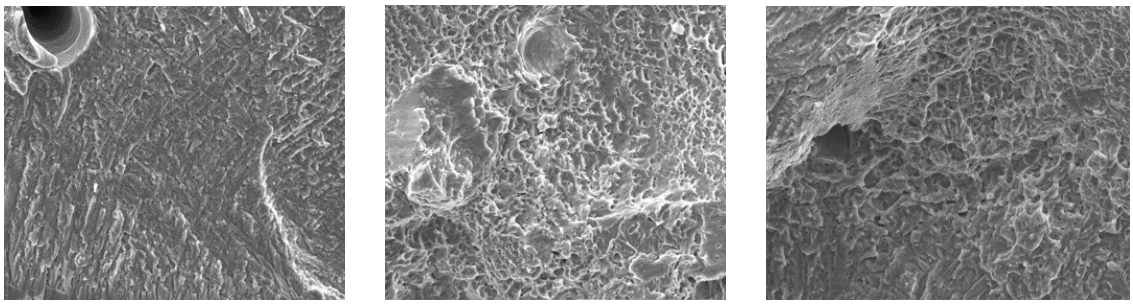

Figure 3.6: Fracture types: Transgranular fracture (left), overload dimple rupture (middle) and the mixed type (right). All of the SEM images belong to tested struts.

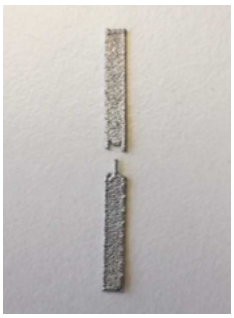

Figure 3.7: Picture of a strut specimen that failed at the transition region.

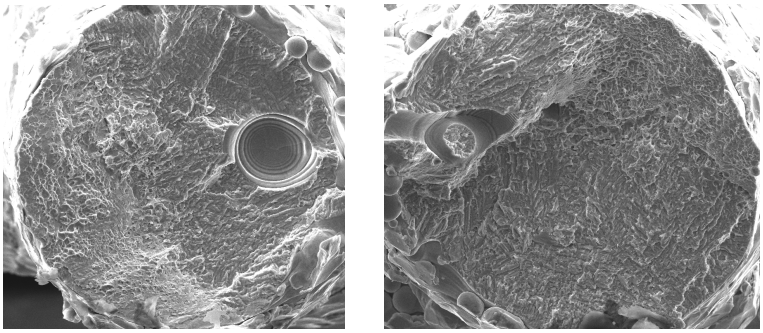

Figure 3.8: Fracture surfaces of a LCF strut (left) and a HCF strut (right).

3.2.2 Lattices

Firstly, it should be mentioned that the individual struts of a lattice mostly failed close to a node, which is due to the higher notch sensitivity in the transition region that leads from the strut to the node. This transition region is equivalent to a notch with a big radius and therefore the fatigue response is very sensitive to these notches.
The fracture behaviors of LCF and HCF lattice specimens have been investigated and compared for the R-ratios R = 0.1 and R = -1. To do this, each fracture surface in the 7 x 7 grid that consists of the nodes of a lattice has been investigated under the SEM. The 7 x 7 grids of some of the lattices with their fracture types is schematically shown in Fig. 3.9. For R = -1, the transgranular fracture type dominated for both lifetime regimes and no differences in fracture behavior between the LCF specimen and the HCF specimen were observed overall [Fig. 3.9 (a) and (b)]. No explanations have been found why the transgranular fracture type dominates for R = -1 and why the fracture type is insensitive to the lifetime. A more detailed study with more specimens is required. For R = 0.1, the amount of transgranular fracture surfaces increased and the number of surfaces that exhibit dimple rupture decreased with increasing lifetime [Fig. 3.9 (c) and (d)].

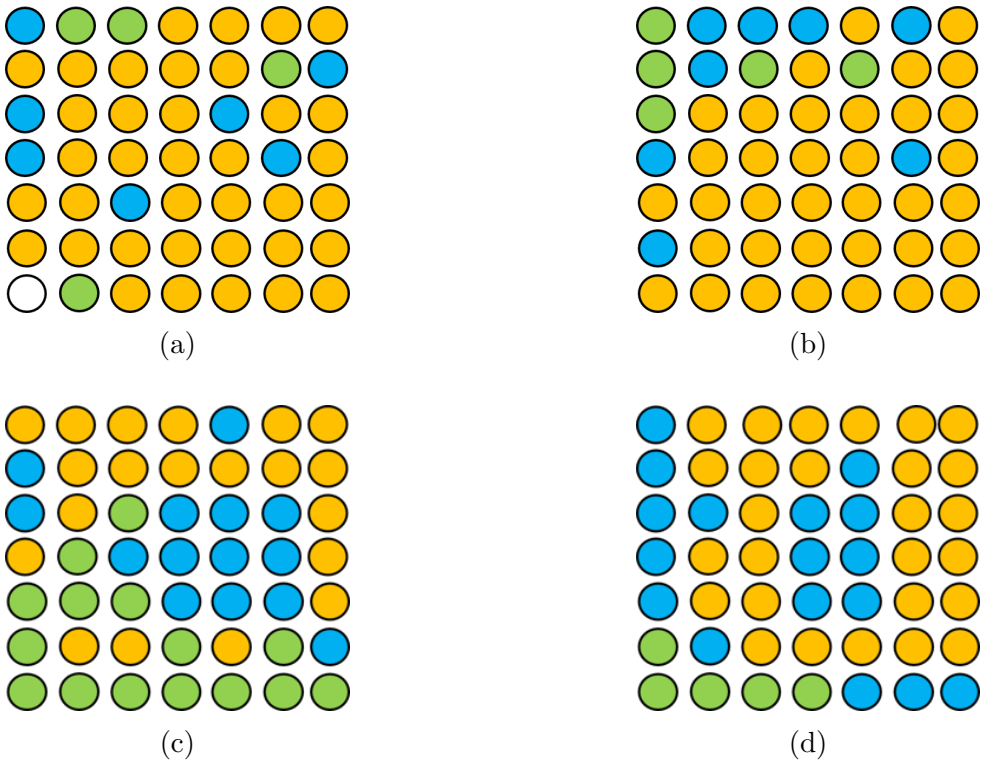

Figure 3.9: Distribution of fracture types in the investigated lattices. Transgranular fracture surfaces are shown in orange, overload dimple rupture surfaces are shown in green and surfaces exhibiting the mixed type are shown in blue. The fracture surface shown in white could not be investigated with the microscope because of pollution. (a) LCF specimen ($N = 9928$), R = -1; (b) HCF specimen ($N = 581100$), R = -1; (c) LCF specimen ($N = 14385$), R = 0.1; (d) HCF specimen ($N = 577475$), R = 0.1.

Chapter 4

Discussion and Outlook

To use Ti-6Al-4V lattices as implants, the structure should be strong enough in fatigue and the prediction of the fatigue performance should not involve a large uncertainty. For the strut specimens that were tested during this project, this uncertainty was large while it was smaller for the lattices. The reason for this might be that fatigue failure of lattices corresponds to the failure of much more struts, making lattices not so sensitive to fatigue response of single individual struts. As-built AM lattices exhibit lower fatigue endurances than traditionally manufactured structures, but this difference could get smaller if the effect of post-treatments and bone ingrowth are taken into account. The post-treatment might remove some of the LOF defects with their unmelted powder particles, which can be harmful to the fatigue strength of the structure. As a conclusion, AM processing and post-processing need further development such that lattice implants with less defects and better fatigue endurances can be fabricated.
As an outlook for future research, I think that the effect of bone ingrowth should be investigated more deeply. To do this, *in vitro* tests need to be performed, but it is very difficult to get access to this kind of tests. The implant should be tested for realistic loading conditions, and to reproduce this situation is not a simple task.

Bibliography

[1] C. Wen-Ming, M. X. Yi, G. Imbalzano, S. Jianhu, X. Shanqing, L. Sung-Jae, P. Vee Sin Lee, "Lattice Ti Structures with Low Rigidity But Compatible Mechanical Strength: Design of Implant Materials for Trabecular Bone", *Int. Journal of Precision Engineering and Manufacturing*, Vol. 17, No. 6, 2016, pp. 793-799.

[2] Li. Guoyuan, W. Lei, P. Wei, Y. Fei, J. Wenbo, W. Xianbo, K. Xiangdong, D. Kerong, H. Yongqiang, "*In vitro* and *in vivo* study of additive manufactured porous Ti6Al4V scaffolds for repairing bone defects", *Scientific Reports 6*, 2016.

[3] M. De Wild, C. Ghayor, S. Zimmermann, J. Rüegg, F. Nicholls, F. Schuler, C. Tse-Hsiang, F. E. Weber "Osteoconductive Lattice Microarchitecture for Optimized Bone Regeneration", *3D Printing and Additive Manufacturing*, vol. 6 , 2019, pp. 40-49.

[4] A. Popovich, V. Sufiiarov, I. Polozov, E. Borisov, D. Masaylo, "Producing hip implants of titanium alloys by additive manufacturing", *Int. Journal of Bioprinting*, vol. 2(2), 2016, pp. 78-84.

[5] S. Arabnejad, R. B. Johnston, J. A. Pura, B. Singh, M. Tanzer, D. Pasini, "High-strength porous biomaterials for bone replacement: A strategy to assess the interplay between cell morphology, mechanical properties, bone ingrowth and manufacturing constraints", *Acta Biomaterialia*, vol. 30, 2016, pp. 345-356.

[6] L. Qianchu, J. Elambasseril, S. Shoujin, M. Leary, M. Brandt, P. K. Sharp, "The Effect of Manufacturing Defects on The Fatigue Behavior of Ti-6Al-4V Specimens Fabricated Using Selective Laser Melting", *Advanced Materials Research*, vols. 891-892, 2014, pp. 1519-1524.

[7] T. Persenot, J. Buffiere, E. Maire, R. Dendievel, G. Martin, "Fatigue properties of EBM as-built and chemically etched thin parts", *Procedia Structural Integrity*, vol. 7, 2017, pp. 158-165.

[8] R. Hedayati, S. Janbaz, M. Sadighi, M. Mohammadi-Aghdam, A. A. Zadpoor, "How does tissue regeneration influence the mechanical behavior of additively manufactured porous biomaterials?", *Journal of the Mechanical Behavior of Biomedical Materials*, vol. 65, 2017, pp. 831-841.

[9] P. Li, D. H. Warner, A. Fatemi, N . Phan, "Critical assessment of the fatigue performance of additively manufactured Ti-6Al-4V and perspective for future research", *International Journal of Fatigue*, vol. 85, 2016, pp. 130-143.

[10] S. Leuders, T. Lieneke, S. Lammers, T. Tröster, T. Niendorf, "On the fatigue properties of metals manufactured by selective laser melting – The role of ductility", *Journal of Materials Research*, vol. 29, 2014, pp. 1911-1919.

[11] G. Kasperovich, J. Hausmann, "Improvement of fatigue resistance and ductility of TiAl6V4 processed by selective laser melting", *Journal of Materials Processing Technology*, vol. 220, 2015, pp. 202-214.